

# Quantitative Evaluation of a Multi-Modal Camera Setup for Fusing Event Data with RGB Images

Julian Moosmann, Jakub Mandula, Philipp Mayer, Luca Benini, Michele Magno  
Dept. of Information Technology and Electrical Engineering, ETH Zürich, Switzerland

**Abstract**—Event-based cameras, also called silicon retinas, potentially revolutionize computer vision by detecting and reporting significant changes in intensity asynchronous events, offering extended dynamic range, low latency, and low power consumption, enabling a wide range of applications from autonomous driving to longtime surveillance. As an emerging technology, there is a notable scarcity of publicly available datasets for event-based systems that also feature frame-based cameras, in order to exploit the benefits of both technologies. This work quantitatively evaluates a multi-modal camera setup for fusing high-resolution dynamic vision sensor (DVS) data with RGB image data by static camera alignment. The proposed setup, which is intended for semi-automatic DVS data labeling, combines two recently released Prophesee EVK4 DVS cameras and one global shutter XIMEA MQ022CG-CM RGB camera. After alignment, state-of-the-art object detection or segmentation networks label the image data by mapping boundary boxes or labeled pixels directly to the aligned events. To facilitate this process, various time-based synchronization methods for DVS data are analyzed, and calibration accuracy, camera alignment, and lens impact are evaluated. Experimental results demonstrate the benefits of the proposed system: the best synchronization method yields an image calibration error of less than 0.90 px and a pixel cross-correlation deviation of 1.6 px, while a lens with 8 mm focal length enables detection of objects with size 30 cm at a distance of 350 m against homogeneous background.

**Index Terms**—Computer vision, dynamic vision sensors (DVS), event-based camera, sensor fusion, edge computing, image alignment, multi-camera setup.

## I. INTRODUCTION

Deep learning and artificial intelligence (AI) have accelerated and changed the way computers process visual information in digital systems [1]. Image classification [2], object detection [3], [4], or semantic segmentation [5] are essential capabilities for autonomous agents with tasks such as localization [6], mapping [7], [8], or navigation [9]. Most algorithms for object detection and semantic segmentation operate on color (RGB) image frames [10]. Notably, these algorithms heavily rely on extensive data for training the underlying neural network (NN) [11]. Unfortunately, the current commercially available charge-coupled device (CCD) and complementary metal-oxide semiconductor (CMOS) sensors struggle with high dynamic range and produce a vast quantity of dense data making the tracking of high-velocity objects in adverse lighting conditions a challenge [12]–[14]. To address this limitation, event-based cameras, also known as silicon retinas, have emerged as a promising bio-inspired branch of image sensors [15], [16]. Dynamic vision sensor (DVS) cameras do not directly measure the absolute intensity of light

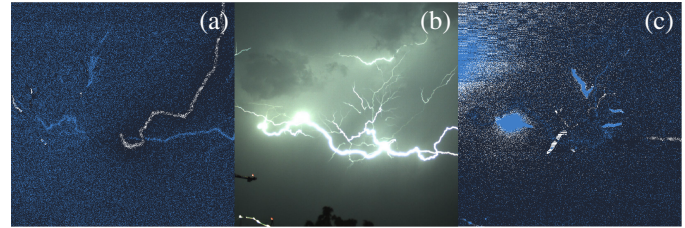


Fig. 1. DVS camera recording a bolt of lightning (a) clear image without saturation. (b) The corresponding RGB image. (c) Shows the sensor saturating and merging events together into spurious line artifacts.

but rather detect and respond to changes in light intensity as seen in Fig. 1. When a DVS pixel detects an intensity change, the camera generates an asynchronous message with the pixel coordinates. This differs from the conventional approach of utilizing a rolling or global shutter mechanism and allows for an exceptional dynamic range [17] of over 86 dB [18] and superior capturing speed [15]. As such the DVS cameras produce highly sparse data, especially in static scenarios.

However, the novelty of the technology results in a scarcity of available labeled datasets containing DVS data [19], and even fewer datasets are available with a dual camera scenario where DVS are combined with RGB cameras. The necessity to create new algorithms that account for time dependencies is approached by two main ideas. A bio-inspired data processing approach using spiking neural networks (SNNs) which requires specialized hardware from the field of mixed analog and digital processing [20]. Or a frame-based approach that allows for the utilization of traditional deep neural networks (DNNs) by accumulating events and integrating them over a certain time period and as such creates a two-dimensional image frame out of event data [21]. This work presents and evaluates a system for DVS dataset collection based on simultaneous recordings of RGB frames and DVS data. Subsequently, postprocessing techniques are utilized to align the RGB and DVS pixels. Once aligned, a state-of-the-art object detection algorithm such as YOLO [22]–[29] is applied to the RGB frames, yielding accurate pixel/box labels that can be transformed onto the DVS camera view as proposed in [30].

The main contributions of the work can be summarized as follows: (i) Investigation of data synchronization methods for frame- and event-based vision sensors, achieving a calibration accuracy with a standard deviation of 0.90 px and projected image cross-correlation deviation of 1.6 px. (ii) Quantitative analysis of object perception by combining DVS sensors with lenses of different focal lengths. (iii) Practical evaluation of

arXiv:2311.01881v1 [eess.IV] 3 Nov 2023

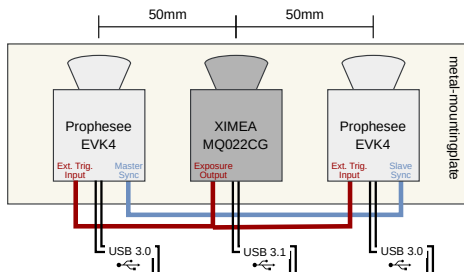


Fig. 2. The proposed hardware setup for data collection includes two Prophesee EVK4 event-based cameras and one Ximea RGB image sensor (MQ022CG-CM) with hardware synchronization. The Ximea outputs a digital signal during its exposure time that is hardware time-stamped into the event stream.

data generation quantity for various vision scenarios for a  $1280 \times 720$  pixels DVS sensor.

## II. CAMERA SETUP

The proposed multi-camera setup (Fig. 2) consists of one frame-based CMOS RGB camera from Ximea (MQ022CG-CM) and two Prophesee EVK4 event cameras—having the largest DVS resolution commercially available—all of which are hardware synchronized to each other. The two Prophesee cameras enable stereo vision capture, however, in this work, different optics were mounted on each camera in order to efficiently compare lenses with various field of views (FoVs). The primary function of the RGB camera is to facilitate semi-automatic labeling, which aids in the creation of event-based datasets. Calibration is utilized to align the various camera views and allow labels to be transformed between them as suggested in [31]. To simplify the subsequent alignment with event data, a global shutter RGB camera has been chosen to mitigate the complications arising from the row-wise reading of pixels in the rolling shutter cameras. In addition to the targeted field of view and the varying-sized camera sensors\*, the lens’ focal lengths had to be carefully chosen in order to closely align the FoV and minimize the distortion. In particular, the lenses were chosen such that the Ximea camera has slightly larger FoV allowing for full coverage of the event camera FoV. Table I outlines the final utilized lenses and Table II the lens combinations.

\*Prophesee: EVK4 has a sensor size of  $1/2.5''$  and a resolution of  $1280 \times 720$  while the Ximea: MQ022CG-CM global shutter CMOS camera has a sensor size of  $2/3''$  and a resolution of  $2048 \times 1088$

TABLE I  
AN OVERVIEW OF THE UTILIZED C-MOUNT LENSES.

| Camera    | Lens                      | Specs         |            |
|-----------|---------------------------|---------------|------------|
|           |                           | Focal length* | Distortion |
| Ximea     | X100 Navitar: MVL100M23   | 100 mm        | 0.05 %     |
|           | X75 Tamron: M112FM75      | 75 mm         | 0.00 %     |
|           | X50 Computar: M5028-MPW3  | 50 mm         | 0.00 %     |
|           | X12.5 Fujinon: HF12.5SA-1 | 12.5 mm       | 0.40 %     |
| Prophesee | P100 Navitar: MVL100M23   | 100(181) mm   | 0.05 %     |
|           | P75 Computar: M7528-MPW3  | 75(136) mm    | 0.12 %     |
|           | P50 Tamron: M117FM50-RG   | 50(91) mm     | 0.01 %     |
|           | P35 Computar: M3528-MPW3  | 35(63) mm     | 0.03 %     |
|           | P8 SOYO: SFA0820-5M       | 8(15) mm      | <0.1 %     |

\* Number in (brackets) is the effective focal length accounting for the sensor’s crop factor.

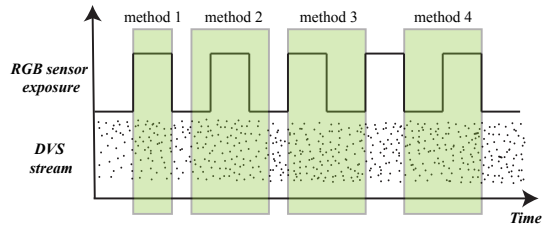


Fig. 3. Visualization of the four ways to synchronize event- with frame-based data. The green windows illustrate which events are integrated and synchronized to an RGB image frame. An RGB image frame is created whenever the RGB sensor exposes, while the DVS creates a continuous data stream.

## III. METHOD

The proposed system undergoes a comprehensive **quantitative analysis**, taking into account factors such as sensor shutters, optical distortions, and influences from camera peripherals. Understanding these technical challenges is crucial for effectively **synchronizing and calibrating** the pixels of the DVS to the RGB data. The evaluation of the synchronization is done by testing four different synchronization methods, visualized in Fig. 3, and comparing the calibration accuracies of the matched camera FoVs on a pixel level Table II. This requires a conversion from the event-based data stream into image frames by accumulating event data over a constant period of time [32], [33]. While the calibration process is carried out using Kalibr [34], utilizing the protocol suggested in [35], the paper lacks reproducible error measurements. To address this gap, the standard deviation of the re-projection error in pixels—reported by Kalibr—is included in this report, allowing for more comprehensive comparisons and evaluations of calibration accuracy. To verify the homography projection accuracy, edges in the two DVS frame and RGB frame views of distant scenes are detected using a Canny filter, and the matching deviation from the center is computed using zero mean normalized cross-correlation (ZNCC) [36]. The estimation of **DVS data quantity** is non-trivial for different backgrounds and camera movement speeds and differs significantly from the data amount created by frame-based sensors. In the case of event data, the IMX636 sensor can produce anywhere from nearly  $0 \text{ Ev/s}$  to  $1 \text{ GEv/s}$  in highly dynamic scenes [18]. However, in practice, the USB peripheral is limited to  $\sim 1.6 \text{ Gbit/s}$  transfer speed, sustaining only about  $115 \text{ MEv/s}$ . Consequently, this work conducts an analysis of data generation that is dependent on the scene, aiming to offer a reference for future considerations in storage design and bandwidth budget. Finally, this work evaluates the perceptible **object size at different distances** with multiple lenses. This goes hand-in-hand with the selection of suitable lenses for the setup. While it may appear to involve solely basic optics calculations, the field measurements point out that small objects have a tendency to disappear, even when their theoretical size should be sufficient for detection. This phenomenon can be attributed to the fact that the object at a distance fails to induce sufficient changes in pixel intensity for the DVS camera to register a data point. This investigation is done for objects traveling with high-speed ( $800 \text{ m/s}$ ) and low to medium-speed ( $0.5 \text{ m/s}$ – $30 \text{ m/s}$ ).

## IV. EXPERIMENTAL RESULTS

The setup introduced in Section II has been analyzed to optimize the synchronization of event-based and frame-based sensors, object perception distances, and expected event data rates. For data collection, the camera system has been connected to a laptop via USB 3.0 and USB 3.1 GEN1 for the Prophesee EVK4 and XIMEA MQ022CG-CM, respectively. It was found that without setting an explicit Event Rate Control (ERC) of 100 MEV/s, frames and events could be lost. This was adjusted for certain scenes where bursts could be tolerated. If there were more events present in the scene, the sensor saturated which manifested in line artifacts, visible in Fig. 1 or in the worst case events being completely dropped.

**A. Calibration accuracy achieved:** This paper exploits the approach proposed in [35] for event camera calibration using Kalibr and reports the calibration accuracy as reprojection error standard deviation to be below 1.6 px. This is significantly worse than what’s possible with Global shutter cameras, which readily feature an error below 0.2 px. Method 1 shown in Fig. 3 proved to generate poor image quality resulting in calibration failing. Methods 2, 3, and 4 had similar performance. As such, the achieved standard deviation error results using only method 2 are displayed in Table II. Notably, the calibration of large focal-length lenses proved to be a challenging task.

**B. Lens vs. object size and distance:** Investigating the objects traveling with different speeds at different distances, a commercial drone (30 cm) at 300 m altitude can be detected on an accumulated DVS frame with up to 12 px using a 35 mm lens as shown in Table III. Against a homogeneous background (sky), the contrast is much greater. The drone is even detectable at an altitude of 350 m using the 8 mm lens despite according to optical calculations only having a size of 1.4 px. However, when investigating fast-traveling objects like bullet shots—with a size of 2 cm—the bullet is lost at <80 m even though it still should be 1 px at a distance of 400 m (using 100mm lens).

TABLE II

LENS COMBINATIONS AND CORRESPONDING CALIBRATION ACCURACIES FOR SYNCHRONIZATION METHODS (SEE FIG. 3), REPRESENTED AS THE STANDARD DEVIATION IN PIXELS.

| Lens Configuration |       |       | Standard Deviation |       |       | Cross-correlation deviation |        |        |
|--------------------|-------|-------|--------------------|-------|-------|-----------------------------|--------|--------|
| DVS-L              | RGB   | DVS-R | DVS-L              | RGB   | DVS-R | Sync 2                      | Sync 3 | Sync 4 |
| P100               | X50   | P50   | 1.589              | 0.797 | 1.279 | 4.1                         | 4.9    | 4.7    |
| P75                | X50   | P35   | 1.279              | 0.696 | 1.016 | 4.4                         | 3.4    | 2.3    |
| P50                | X12.5 | P8    | 0.768              | 0.493 | 1.254 | 2.1                         | 3.3    | 2.9    |
| P35                | X12.5 | P8    | 0.665              | 0.494 | 0.900 | 2.2                         | 3.4    | 1.6    |

TABLE III

OBJECT RESOLUTION USING THE DVS AT DIFFERENT DISTANCES USING A SELECTION OF LENSES.

| Object                   | Distance | 8mm lens |                    | 35mm lens |       | 100mm lens |       |
|--------------------------|----------|----------|--------------------|-----------|-------|------------|-------|
|                          |          | Theory   | Meas.              | Theory    | Meas. | Theory     | Meas. |
| Drone 30 cm              | 100m     | 5 px     | 5 px               | 22 px     | 20 px | 61 px      | -     |
| Drone 30 cm              | 300m     | 1.6 px   | ND                 | 7 px      | 8 px  | 20 px      | -     |
| Drone <sup>‡</sup> 30 cm | 350m     | 1.4 px   | ~3 px <sup>‡</sup> | 6 px      | ~7 px | 18 px      | -     |
| Bullet 2 cm              | 10m      | 3 px     | 3 px               | 14 px     | -     | 41 px      | 38 px |
| Bullet 2 cm              | 30m      | 1 px     | ND                 | 5 px      | 1 px  | 14 px      | 1 px  |
| Bullet 2 cm              | 100m     | 0.3 px   | ND                 | 1.4 px    | ND    | 4 px       | 1 px  |
| Bullet 2 cm              | 400m     | 0.08 px  | ND                 | 0.35 px   | ND    | 1 px       | ND    |

<sup>‡</sup> Drone with homogeneous blue-white sky background.  
ND: in configurations where the object is not detectable.

TABLE IV

THE AVERAGE DATA RATE CREATED BY THE PROPHESSEE EVK4 DVS CAMERAS FOR DIFFERENT SCENERY AND CAMERA SETUP SCENARIOS.

| Scenery    | Obj. Size | Camera motion |           |                            |
|------------|-----------|---------------|-----------|----------------------------|
|            |           | Static        | Dynamic   | Dynamic - Sky <sup>‡</sup> |
| Drone Near | 30 cm     | 20 MB/s       | 70 MB/s   | 36 MB/s                    |
| Drone Far  | 30 cm     | 0.5 MB/s      | 70 MB/s   | 3 MB/s                     |
| Car        | 3 m       | 15 MB/s       | 100 MB/s  | -                          |
| Shots      | 2 cm      | 0.1 MB/s      | 60 MB/s   | -                          |
| Explosion  | 5 m       | *450 MB/s     | -         | -                          |
| Rain       | -         | 160 MB/s      | *360 MB/s | 10 MB/s                    |

\* Peak value before saturation reached

<sup>‡</sup> Object with homogeneous sky background

**C. Data amount vs. moving DVS camera:** As described in the method Section III, the amount of data created is non-trivial to calculate. Therefore baseline measurements for a static camera and dynamic camera (panning at  $\leq 0.25$  rad/s) are reported, measuring bullet shots, flying drones and vehicles, on a homogeneous (sky) and non-homogeneous background (mountain and grass), see Table IV. Notably, the dynamic camera produces orders of magnitude more data. However, homogeneous backgrounds, such as the sky, can significantly reduce the number of context events. The highest data rate without reaching saturation is 180 MB/s. However, for short bursts, the sensor can reach a peak rate of 400 MB/s, which is the maximal rate set in the ERC. For comparison, the Ximea frame camera recording in 10-bit RAW generates 260 MB/s continuously.

**D. System limitation:** Last but not least, some limitations of the DVS cameras are presented. Most notably, insects and non-homogeneous background movements (e.g. wind moving trees) can create a significant number of irrelevant events. Scenes with brief abrupt changes in light intensity, such as explosions, lightning, strobe lights, or motion can temporarily overwhelm the sensor; sometimes resulting in complete data loss. In particular, the rain proved a significant challenge often causing camera saturation.

## V. CONCLUSION

This work presented a multi-modal camera setup for semi-automated collection and labeling of DVS data. This included the analysis of various event-to-RGB image frame synchronization techniques, and corresponding calibration accuracy and pixel cross-correlation are reported. Measurement results show that lenses with similar FoV and low distortion achieve a calibration accuracy of less than 0.90 px, with a corresponding pixel cross-correlation of 1.6 px. Furthermore, tests demonstrated that an object of a size of 30 cm on the homogeneous background can still be detected at a distance of 350 m, using the Prophesee EVK4 sensor with a wide 8 mm lens. In-field experience of the data bandwidth ranges from 0.1 MB/s - 20 MB/s for static camera recordings while a moving DVS camera generates data in the order of 350 MB/s.

## ACKNOWLEDGMENTS

The authors would like to thank armasuisse Science & Technology and RUAG Ltd. for funding this research.

## REFERENCES

- [1] J. Chai, H. Zeng, A. Li, and E. W. T. Ngai, "Deep learning in computer vision: A critical review of emerging techniques and application scenarios," *Machine Learning with Applications*, vol. 6, p. 100134, Dec. 2021, doi: 10.1016/j.mlwa.2021.100134.
- [2] L. Chen, S. Li, Q. Bai, J. Yang, S. Jiang, and Y. Miao, "Review of image classification algorithms based on convolutional neural networks," *Remote Sensing*, vol. 13, no. 22, p. 4712, 2021, doi: 10.3390/rs13224712.
- [3] N. Carion, F. Massa, G. Synnaeve, N. Usunier, A. Kirillov, and S. Zagoruyko, "End-to-End Object Detection with Transformers," *arXiv*, 2020, doi: 10.48550/arXiv.2005.12872.
- [4] W. Liu *et al.*, "SSD: Single shot MultiBox detector," in *Computer Vision – ECCV 2016*, 2016, pp. 21–37, doi: 10.1007/978-3-319-46448-0\_2.
- [5] J. Long, E. Shelhamer, and T. Darrell, "Fully convolutional networks for semantic segmentation," in *2015 IEEE Conference on Computer Vision and Pattern Recognition (CVPR)*, Los Alamitos, CA, USA, jun 2015, pp. 3431–3440, doi: 10.1109/CVPR.2015.7298965.
- [6] N. Zimmerman, T. Guadagnino, X. Chen, J. Behley, and C. Stachniss, "Long-Term Localization Using Semantic Cues in Floor Plan Maps," *IEEE Robotics and Automation Letters*, vol. 8, no. 1, pp. 176–183, 2023, doi: 10.1109/LRA.2022.3223556.
- [7] A. Rosinol, M. Abate, Y. Chang, and L. Carlone, "Kimera: an Open-Source Library for Real-Time Metric-Semantic Localization and Mapping," in *2020 IEEE International Conference on Robotics and Automation (ICRA)*, 2020, pp. 1689–1696, doi: 10.1109/ICRA40945.2020.9196885.
- [8] N. Zimmerman, M. Sodano, E. Marks, J. Behley, and C. Stachniss, "Long-Term Indoor Localization with Metric-Semantic Mapping using a Floor Plan Prior," *arXiv*, 2023, doi: 10.48550/arXiv.2303.10959.
- [9] J. Crespo, J. C. Castillo, O. M. Mozos, and R. Barber, "Semantic Information for Robot Navigation: A Survey," *Applied Sciences*, vol. 10, no. 2, 2020, doi: 10.3390/app10020497.
- [10] W. Liu, Z. Wang, X. Liu, N. Zeng, Y. Liu, and F. E. Alsaadi, "A survey of deep neural network architectures and their applications," *Neurocomputing*, vol. 234, pp. 11–26, 2017, doi: 10.1016/j.neucom.2016.12.038.
- [11] X. Zhu, C. Vondrick, C. C. Fowlkes, and D. Ramanan, "Do we need more training data?" *International Journal of Computer Vision*, vol. 119, no. 1, pp. 76–92, 2016, doi: 10.1007/s11263-015-0812-2.
- [12] A. El Gamal and H. Eltoukhy, "CMOS image sensors," *IEEE Circuits and Devices Magazine*, vol. 21, no. 3, pp. 6–20, 2005, doi: 10.1109/MCD.2005.1438751.
- [13] M. Hillebrand, N. Stevanovic, B. Hosticka, J. Santos Conde, A. Teuner, and M. Schwarz, "High speed camera system using a CMOS image sensor," in *Proceedings of the IEEE Intelligent Vehicles Symposium 2000*, 2000, pp. 656–661, doi: 10.1109/IVS.2000.898423.
- [14] W.-C. Kao, C.-C. Hsu, L.-Y. Chen, C.-C. Kao, and S.-H. Chen, "Integrating image fusion and motion stabilization for capturing still images in high dynamic range scenes," *IEEE Transactions on Consumer Electronics*, vol. 52, no. 3, pp. 735–741, Aug. 2006, doi: 10.1109/TCE.2006.1706464, Conference Name: IEEE Transactions on Consumer Electronics.
- [15] G. Gallego *et al.*, "Event-Based Vision: A Survey," *IEEE Transactions on Pattern Analysis and Machine Intelligence*, vol. 44, no. 01, pp. 154–180, jan 2022, doi: 10.1109/TPAMI.2020.3008413.
- [16] X. Zheng *et al.*, "Deep learning for event-based vision: A comprehensive survey and benchmarks," *arXiv*, 2023, doi: 10.48550/arXiv.2302.08890.
- [17] P. Lichtsteiner, C. Posch, and T. Delbrück, "A 128 × 128 120 dB 15 μs Latency Asynchronous Temporal Contrast Vision Sensor," *IEEE Journal of Solid-State Circuits*, vol. 43, no. 2, pp. 566–576, 2008, doi: 10.1109/JSSC.2007.914337.
- [18] "Event-based Vision Sensor (EVS) | Products & Solutions," [Online]. Available: <https://www.sony-semicon.com/en/products/is/industry/evs.html>.
- [19] A. Lakshmi, A. Chakraborty, and C. S. Thakur, "Neuromorphic vision: From sensors to event-based algorithms," *Wiley Interdisciplinary Reviews: Data Mining and Knowledge Discovery*, vol. 9, no. 4, p. e1310, 2019, doi: 10.1002/widm.1310.
- [20] S. Negi, D. Sharma, A. K. Kosta, and K. Roy, "Best of Both Worlds: Hybrid SNN-ANN Architecture for Event-based Optical Flow Estimation," Jun. 2023, arXiv:2306.02960 [cs]. [Online]. Available: <http://arxiv.org/abs/2306.02960>.
- [21] A. I. Maqueda, A. Loquercio, G. Gallego, N. Garcia, and D. Scaramuzza, "Event-based Vision meets Deep Learning on Steering Prediction for Self-driving Cars," in *2018 IEEE/CVF Conference on Computer Vision and Pattern Recognition*, Jun. 2018, pp. 5419–5427, doi: 10.1109/CVPR.2018.00568, ArXiv:1804.01310 [cs].
- [22] J. Redmon, S. Divvala, R. Girshick, and A. Farhadi, "You Only Look Once: Unified, Real-Time Object Detection," in *2016 IEEE Conference on Computer Vision and Pattern Recognition (CVPR)*, 2016, pp. 779–788, doi: 10.1109/CVPR.2016.91.
- [23] J. Redmon and A. Farhadi, "YOLO9000: Better, Faster, Stronger," in *2017 IEEE Conference on Computer Vision and Pattern Recognition (CVPR)*, 2017, pp. 6517–6525, doi: 10.1109/CVPR.2017.690.
- [24] J. Redmon and A. Farhadi, "Yolov3: An incremental improvement," *arXiv*, 2018, doi: 10.48550/arXiv.1804.02767.
- [25] A. Bochkovskiy, C.-Y. Wang, and H.-Y. M. Liao, "Yolov4: Optimal speed and accuracy of object detection," *arXiv*, 2020, doi: 10.48550/arXiv.2004.10934.
- [26] G. Jocher, "YOLOv5 by Ultralytics," *github*, 2020, doi: 10.5281/zenodo.3908559.
- [27] C. Li *et al.*, "YOLOv6: A single-stage object detection framework for industrial applications," *arXiv*, 2022, doi: 10.48550/arXiv.2209.02976.
- [28] C.-Y. Wang, A. Bochkovskiy, and H.-Y. M. Liao, "YOLOv7: Trainable bag-of-freebies sets new state-of-the-art for real-time object detectors," in *Proceedings of the IEEE/CVF Conference on Computer Vision and Pattern Recognition*, 2023, pp. 7464–7475, doi: 10.48550/arXiv.2207.02696.
- [29] G. Jocher, A. Chaurasia, and J. Qiu, "YOLO by Ultralytics," *github*, 2023, <https://github.com/ultralytics/ultralytics>.
- [30] E. Perot, P. de Tournemire, D. Nitti, J. Masci, and A. Sironi, "Learning to Detect Objects with a 1 Megapixel Event Camera," in *Proceedings of the 34th International Conference on Neural Information Processing Systems*, ser. NIPS'20, Red Hook, NY, USA, 2020.
- [31] P. de Tournemire, D. Nitti, E. Perot, D. Migliore, and A. Sironi, "A Large Scale Event-based Detection Dataset for Automotive," *arXiv*, 2020, doi: 10.48550/arXiv.22001.08499.
- [32] H. Rebecq, R. Ranftl, V. Koltun, and D. Scaramuzza, "Events-To-Video: Bringing Modern Computer Vision to Event Cameras," *2019 IEEE/CVF Conference on Computer Vision and Pattern Recognition (CVPR)*, pp. 3852–3861, 2019, doi: 10.1109/CVPR.2019.00398.
- [33] H. Rebecq, R. Ranftl, V. Koltun, and D. Scaramuzza, "High Speed and High Dynamic Range Video with an Event Camera," *IEEE Transactions on Pattern Analysis and Machine Intelligence*, vol. 43, no. 6, pp. 1964–1980, 2019, doi: 10.1109/TPAMI.2019.2963386.
- [34] P. Furgale, J. Rehder, and R. Siegwart, "Unified temporal and spatial calibration for multi-sensor systems," in *2013 IEEE/RSJ International Conference on Intelligent Robots and Systems*, 2013, pp. 1280–1286, doi: 10.1109/IROS.2013.6696514.
- [35] M. Muglikar, M. Gehrig, D. Gehrig, and D. Scaramuzza, "How to Calibrate Your Event Camera," 2021.
- [36] L. Di Stefano, S. Mattoccia, and F. Tombari, "ZNCC-based template matching using bounded partial correlation," *Pattern Recognition Letters*, vol. 26, pp. 2129–2134, Oct. 2005, doi: 10.1016/j.patrec.2005.03.022.